Journal of Alloys and Compounds 509 (2011) 2164–2169

Contents lists available at ScienceDirect

Journal of Alloys and Compounds

journal homepage: www.elsevier.com/locate/jallcom

Growth, thermal and polarized spectral properties of Nd^{3+}-doped $Li_3Ba_2Gd_3(MoO_4)_8$ crystal

Mingjun Song[a,*], Wang Zhao[b], Guofu Wang[c], Meili Zhao[a], Lintong Wang[a]

[a] College of Chemistry and Chemical Engineering, Weifang University, Weifang, Shandong 261061, China
[b] Department of Physics, Huainan Normal University, Huainan, Anhui 232001, China
[c] Fujian Institute of Research on the Structure of Matter, The Chinese Academy of Sciences, Fuzhou, Fujian 350002, China

ARTICLE INFO

Article history:
Received 5 July 2010
Received in revised form 27 October 2010
Accepted 28 October 2010
Available online 9 November 2010

Keywords:
Optical materials
Crystal growth
Optical properties
Thermal expansion

ABSTRACT

Nd^{3+}:$Li_3Ba_2Gd_3(MoO_4)_8$ crystal has been grown from a Li_2MoO_4 flux by the top seed solution growth method (TSSG). The structure of the crystal was confirmed by X-ray powder diffraction. The principal coefficients of thermal expansion along *a*, *b* and *c*-axes were precisely measured to be 1.62×10^{-5}, 1.73×10^{-5} and 2.15×10^{-5} K^{-1}, respectively. The specific heat value was 0.42 J/g K at 50 °C. The polarized spectral properties of Nd^{3+}:$Li_3Ba_2Gd_3(MoO_4)_8$ crystal were investigated and the spectroscopic parameters were calculated and analyzed based on the Judd–Ofelt theory. The absorption cross-sections around 805 nm were determined to be 15.13, 3.84 and 5.27×10^{-20} cm^2 for E//*b*, E//*D*1 and E//*D*2, respectively. The emission cross-sections σ_{em} were determined to be 9.5×10^{-20} cm^2 for E//*b*, 8.2×10^{-20} cm^2 for E//*D*1, and 7.9×10^{-20} cm^2 for E//*D*2, respectively. The fluorescence lifetime was measured to be 130 μs and the quantum efficiency was calculated to be 93%.

1. Introduction

The development of diode-pumped solid-state lasers has found a wide variety of applications in military, industry, medical treatment and scientific research. Therefore, considerable attention has been devoted to the search for new more efficient materials for pumping [1–10]. Among the reported crystals, some molybdate crystals with disordered structure have generated a great deal of interest due to their intriguing properties such as high damage threshold, wide absorption band and high quantum efficiency which made them promising materials for solid-state laser gain media [11–16].

The $Li_3Ba_2Gd_3(MoO_4)_8$ crystal, a member of $Li_3Ba_2Ln_3(MoO_4)_8$ (Ln = La–Lu, Y) family, belongs to the monoclinic system with space group *C*2/*c* and a disordered structure [17,18]. Previously, we have successfully grown large and high-quality $Li_3Ba_2Gd_3(MoO_4)_8$ crystals and reported the spectroscopic properties of Nd^{3+}-doped $Li_3Ba_2Gd_3(MoO_4)_8$ crystal [19]. The results show that Nd^{3+}:$Li_3Ba_2Gd_3(MoO_4)_8$ crystal exhibits excellent spectroscopic properties and could be regarded as a potential solid-state laser crystal material. However, for a proper evaluating of its laser performances and designing its best laser operating conditions, it is necessary to get the detailed and complete information about the polarized spectroscopic properties. Besides, the thermal properties of the crystals, such as thermal expansion coefficient and specific heat, are also very important for crystal growth and application. Therefore, this paper further reports on the thermal and polarized spectroscopic properties of Nd^{3+}-doped $Li_3Ba_2Gd_3(MoO_4)_8$ crystal.

2. Experimental procedures

2.1. Crystal growth and orientation

Since the incongruent melting behavior of $Li_3Ba_2Gd_3(MoO_4)_8$ crystal prevented the use of the Czochralski method [17,18], the crystal growth was performed by the conventional top seeded solution growth method (TSSG) from a flux of Li_2MoO_4. In order to obtain the optimal composition of solution, the solubility curve of $Li_3Ba_2Gd_3(MoO_4)_8$ crystal in the $Li_3Ba_2Gd_3(MoO_4)_8$–Li_2MoO_4 solution was determined by means of trial seeding. The saturation temperatures were determined for various compositions in the range of 71–87.5 mol% Li_2MoO_4 by adjusting the temperature of the solution until a trial seeding showed no change in weight or surface microtopography after 6–8 h immersion.

The crystal growth was carried out in a vertical tubular muffle furnace with a nickel–chrome wire as a heating element. An AL-708 controller was used to control accurately the furnace temperature and the cooling rate. The starting materials 4 at.% Nd^{3+}-doped $Li_3Ba_2Gd_3(MoO_4)_8$ and Li_2MoO_4 were weighed, with a molar ratio of $NdLi_3Ba_2Gd_3(MoO_4)_8$:Li_2MoO_4 = 1:4. The single-crystalline bars cut perpendicularly to the (0 1 0) face were used as seeds. The crystal was grown at a cooling rate of 1 °C/day and a rotating rate of 12 rpm. Detailed growth procedures can be found in Ref. [20].

Since the $Li_3Ba_2Gd_3(MoO_4)_8$ crystal is biaxial, the three principal axes of the optical indicatrix should be determined before the polarized spectral measurement. In the monoclinic system, one of the principal axes is collinear with the crystallographic *b*-axis and the other two principal axes are perpendicular and position at

* Corresponding author. Tel.: +86 536 8785283; fax: +86 536 8785136.
E-mail address: smj521@hotmail.com (M. Song).

0925-8388/$ – see front matter © 2010 Elsevier B.V. All rights reserved.
doi:10.1016/j.jallcom.2010.10.175

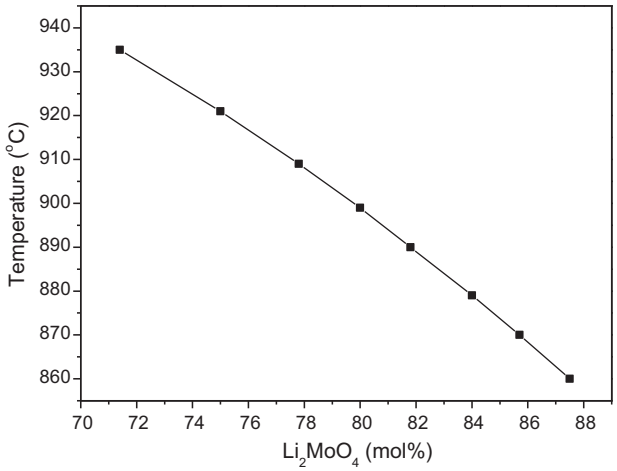

Fig. 1. Solubility curve of $Li_3Ba_2Gd_3(MoO_4)_8$ in $Li_3Ba_2Gd_3(MoO_4)_8$–Li_2MoO_4 solution.

certain angles with respect to crystallographic *a* and *c*-axes. Therefore, the other two principal axes can be easily determined by means of a polarized microscope (PLM).

2.2. Characterization

The X-ray power diffraction pattern of Nd^{3+}:$Li_3Ba_2Gd_3(MoO_4)_8$ crystal was recorded using a D/max-rA type diffractometer equipped with a Cu Kα radiation (λ = 1.54056 Å) in a range of 2θ = 5–85°. The accurate concentration of Nd^{3+} ions in the crystal was determined by the inductively coupled plasma atomic emission spectrometry (ICP-AES) method. The specific heat curve of Nd^{3+}:$Li_3Ba_2Gd_3(MoO_4)_8$ crystal was measured by a NETZSCH DSC 404C simultaneous thermal analyzer at a heating rate of 5 °C/min. The thermal expansion coefficients were measured using a DIL 402PC thermal dilatometer instrument in the range of 325–1050 K.

The polarized absorption spectra were measured using a Perkin–Elmer UV–Vis–NIR spectrometer (Lambda-900) in a wavelength range of 300–1000 nm. The polarized fluorescence spectra and the fluorescence decay curves were measured using an Edinburgh Instruments FLS920 spectrophotometer. All the measurements were carried out at room temperature.

3. Results and discussion

3.1. Crystal appearance and its XRD analysis

By means of trial seeding, the solubility curve of $Li_3Ba_2Gd_3(MoO_4)_8$ crystal in the $Li_3Ba_2Gd_3(MoO_4)_8$–Li_2MoO_4 solution was obtained, as shown in Fig. 1. According to Fig. 1, $Li_3Ba_2Gd_3(MoO_4)_8$ crystal in Li_2MoO_4 flux has a high solubility and large growing temperature region. The as-grown Nd^{3+}:$Li_3Ba_2Gd_3(MoO_4)_8$ crystal with a perfect appearance and well-developed faces is shown in Fig. 2, where the growing orientation of the crystal is along with [0 1 0] direction, and the directions of *a* and *c* axes have been determined by PLM measurement. The directions of the three principal axes with respect to the crystallographic axes are also shown in Fig. 2. Generally, the three principal axes should be named as *X*, *Y*, *Z* in the order of increasing refractive index. However, due to the lack of equipment for precise refractive index measurement, the other two axes perpendicular to the *b*-axis are named as *D*1 and *D*2 temporarily just for convenience of calculation.

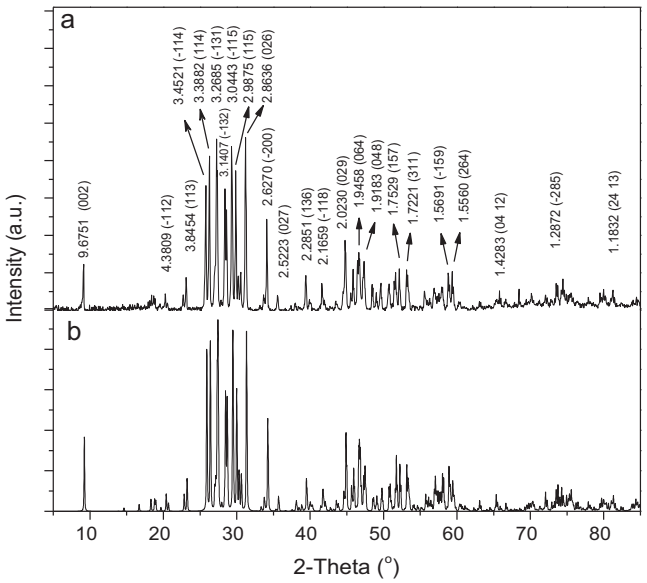

Fig. 3. Comparison of the X-ray powder diffractometer patterns of (a) Nd^{3+}:$Li_3Ba_2Gd_3(MoO_4)_8$ and (b) pure $Li_3Ba_2Gd_3(MoO_4)_8$ crystals.

The XRD patterns of Nd^{3+}:$Li_3Ba_2Gd_3(MoO_4)_8$ crystal is shown in Fig. 3 and compared with that of pure $Li_3Ba_2Gd_3(MoO_4)_8$ crystal. It can be found that the positions and relative intensities of the diffraction peaks are consistent with those of the pure $Li_3Ba_2Gd_3(MoO_4)_8$ crystal on the powder standard (JCPDS-ICDD, No. 77-0830) card. The strong diffraction peaks of Nd^{3+}:$Li_3Ba_2Gd_3(MoO_4)_8$ crystal were indexed and the results showed that the grown Nd^{3+}:$Li_3Ba_2Gd_3(MoO_4)_8$ crystal had the same structure as the pure one. The concentration of Nd^{3+} ions in the grown crystal was determined to be 3.3 at.% by the ICP-AES. Thus, the segregation coefficient of Nd^{3+} ions in the Nd^{3+}:$Li_3Ba_2Gd_3(MoO_4)_8$ crystal was estimated to be 0.82.

3.2. Thermal properties

The specific heat is an important thermal factor that influences the laser damage threshold of a crystal. Generally, the higher the specific is, the larger the laser damage threshold is. Fig. 4 shows the dependence curve of the specific heat on the temperature in the range of 323–675 K. The specific heat increases almost linearly with the increasing temperature. The specific heat value at 323 K is 0.42 J/g K (205.2 cal/mol K), which is close to the values of Nd^{3+}:$YbVO_4$ (0.45 J/g K) and Nd^{3+}:YVO_4 (0.50 J/g K) [21,22]. This indicates that

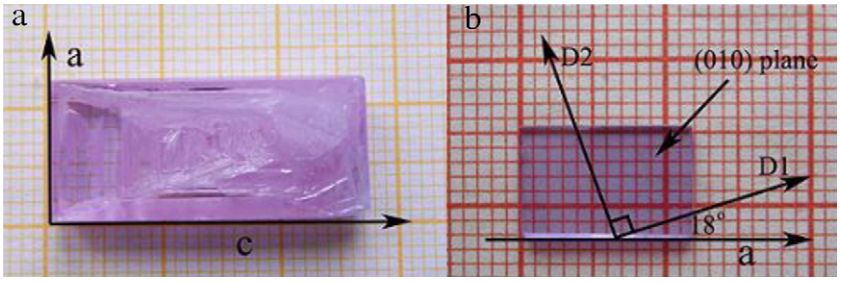

Fig. 2. Grown crystal of Nd^{3+}:$Li_3Ba_2Gd_3(MoO_4)_8$: (a) grown crystal; (b) polished sample with (0 1 0) plane perpendicular to the paper.

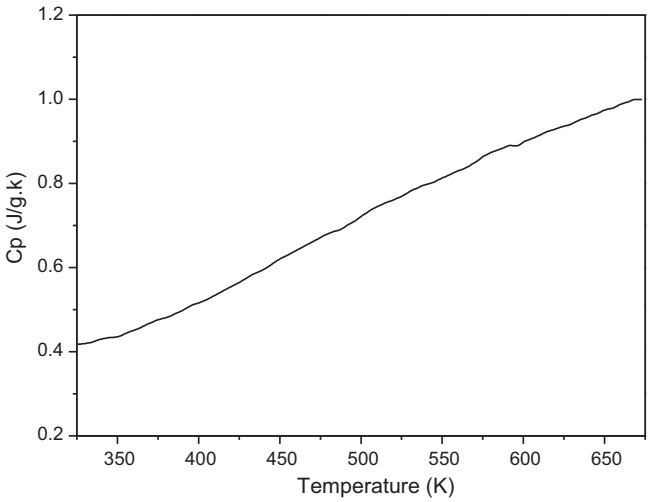

Fig. 4. The dependence of the specific heat of Nd^{3+}:$Li_3Ba_2Gd_3(MoO_4)_8$ crystals on temperature.

Nd^{3+}:$Li_3Ba_2Gd_3(MoO_4)_8$ crystal has a high laser damage threshold.

The thermal expansion coefficient is another important thermal factor for the crystal. As a significant part of the power pump is converted into heat inside the material during laser operation, which will degrade the laser performance, it is important to know its linear thermal expansion coefficients to predict how the material behaves when the temperature increases [23]. The figure of linear expansions versus temperature is shown in Fig. 5. The linear thermal expansion coefficient is defined as:

$$\alpha = \frac{1}{L_0}\frac{\Delta L}{\Delta T} \quad (1)$$

where L_0 is the initial length of the sample at room temperature and ΔL is the change in length when the temperature changes ΔT. We can calculate the thermal expansion coefficients based on the slope of the linear fitting of the linear relationship between $\Delta L/L_0$ and the temperature. In this case, the thermal expansion coefficients along *a*, *b* and *c*-axes are 1.62×10^{-5}, 1.73×10^{-5} and $2.15 \times 10^{-5}\,K^{-1}$, respectively. The result shows that Nd^{3+}:$Li_3Ba_2Gd_3(MoO_4)_8$ crystal has a strong thermal expansion anisotropy. Therefore, in order to obtain Nd^{3+}:$Li_3Ba_2Gd_3(MoO_4)_8$ crystals with free crack, the seed

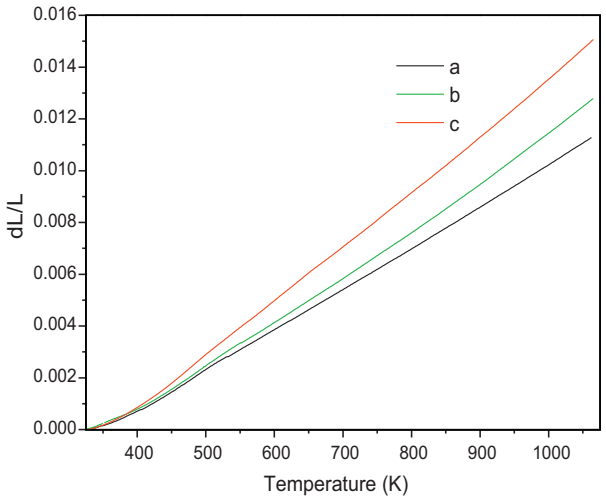

Fig. 5. Thermal expansions of Nd^{3+}:$Li_3Ba_2Gd_3(MoO_4)_8$ crystal along the *a*-, *b*- and *c*-axes.

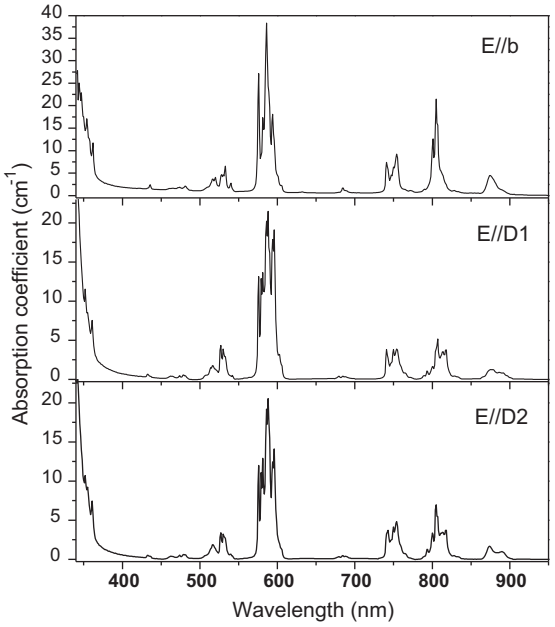

Fig. 6. Polarized absorption spectra of Nd^{3+}:$Li_3Ba_2Gd_3(MoO_4)_8$ at room temperature.

with [0 1 0] orientation and slow annealing rate were applied in the crystal growth procedure.

3.3. Absorption spectra and Judd–Ofelt analysis

Fig. 6 shows the polarized absorption spectra of the Nd^{3+}:$Li_3Ba_2Gd_3(MoO_4)_8$ crystal. The absorption spectra show polarized dependence due to the anisotropy of the crystal and the absorption coefficient for E//*b* is much lager than those of E//*D*1 and E//*D*2. The most interesting feature in the absorption spectra is the broad absorption band around 800 nm, which coincides with the wavelength of radiation from AlGaAs diode laser. Fig. 7 shows the absorption cross-sections for the three polarizations in the region of 720–920 nm for clarity. The absorption cross-sections for E//*D*1 and E//*D*2 at 805 nm are 3.84 and 5.27×10^{-20} cm^2 respectively. The absorption cross-section at 805 nm for E//*b* is 15.13×10^{-20} cm^2, which is the largest among the three directions. This value is smaller than that of Nd^{3+}:YVO_4 (38.7×10^{-20} cm^2 for π polarization) [24]

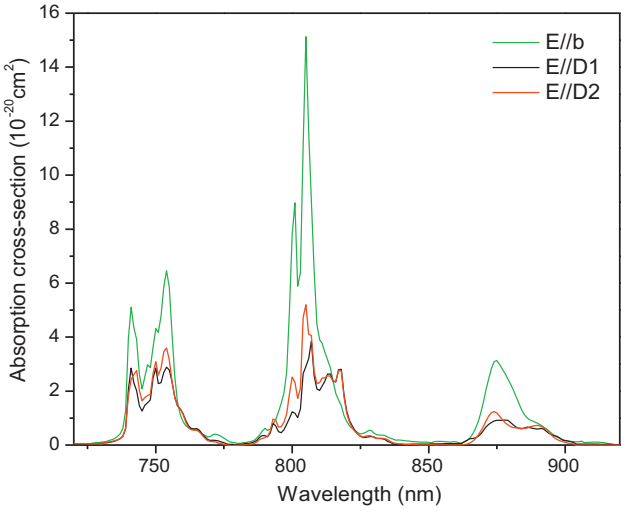

Fig. 7. Polarized absorption cross-sections of Nd^{3+}:$Li_3Ba_2Gd_3(MoO_4)_8$ crystals in a range of 720–920 nm.

Table 1
The measured and calculated line strengths of Nd^{3+}:$Li_3Ba_2Gd_3(MoO_4)_8$ crystal.

Excited state	E//b		E//$D1$		E//$D2$	
	S_{meas} (10^{-20} cm^2)	S_{cal} (10^{-20} cm^2)	S_{meas} (10^{-20} cm^2)	S_{cal} (10^{-20} cm^2)	S_{meas} (10^{-20} cm^2)	S_{cal} (10^{-20} cm^2)
$^4F_{3/2}$	2.596	2.883	1.179	1.265	1.168	1.311
$^4F_{5/2}+{}^2H_{9/2}$	6.456	6.527	3.398	3.504	3.775	3.710
$^4F_{7/2}+{}^4S_{3/2}$	5.206	5.218	3.111	3.069	3.246	3.304
$^4F_{9/2}$	0.377	0.416	0.259	0.238	0.224	0.254
$^4G_{5/2}+{}^2G_{7/2}$	26.578	26.608	21.297	21.310	21.239	21.246
$^2K_{13/2}+{}^4G_{7/2}+{}^4G_{9/2}$	5.072	4.618	2.987	2.778	2.923	2.837
$^2K_{15/2}+{}^2G_{9/2}+{}^2D_{3/2}+{}^4G_{11/2}$	0.917	0.759	0.487	0.374	0.487	0.390
$^2P_{1/2}+{}^2D_{5/2}$	0.311	0.416	0.240	0.227	0.202	0.180
rmsΔS (10^{-21} cm^2)	2.58		1.25		0.96	
rms error (%)	2.6		1.6		1.2	

Table 2
The Judd–Ofelt intensity parameters of Nd^{3+}:$Li_3Ba_2Gd_3(MoO_4)_8$ crystal.

Polarizations	Ω_2 (10^{-20} cm^2)	Ω_4 (10^{-20} cm^2)	Ω_6 (10^{-20} cm^2)
E//b	20.207	10.864	7.139
E//$D1$	18.854	4.483	4.318
E//$D2$	18.691	4.601	4.667
Ω_{eff}	19.251	6.649	5.375

Table 3
The transition probabilities and branch ratios for the $^4F_{3/2} \rightarrow {}^4I_j$ transitions of Nd^{3+}:$Li_3Ba_2Gd_3(MoO_4)_8$ crystal.

Tansitions	E//b		E//$D1$		E//$D2$	
	A (s^{-1})	β	A (s^{-1})	β	A (s^{-1})	β
$^4F_{3/2} \rightarrow {}^4I_{9/2}$	5305	0.502	2328	0.442	2413	0.434
$^4F_{3/2} \rightarrow {}^4I_{11/2}$	4432	0.419	2427	0.461	2594	0.467
$^4F_{3/2} \rightarrow {}^4I_{13/2}$	798	0.075	482	0.092	522	0.094
$^4F_{3/2} \rightarrow {}^4I_{15/2}$	41	0.004	25	0.005	27	0.005
τ_{rad} (μs)						140

but large than that of Nd^{3+}:YAG (7.3×10^{-20} cm^2) [25]. Moreover, the full width at half the maximum (FWHM) of the absorption band is 6 nm for E//b. Such a large line-width is suitable for diode pumping; since it is not crucial to temperature stability of the output wavelength of diode laser.

The Judd–Ofelt (J–O) theory has been mostly used in the analysis of the spectroscopic properties of the rare-earth ions doped crystals and glasses [26,27]. Based on the J–O theory, the data of absorption spectra can be used to calculate the oscillator strength parameters, the radiative lifetime, and the fluorescence branching ratios. First, the line strength of the electric-dipole transition from the ground state $^4I_{9/2}$ to the excited multiplet can be calculated from the corresponding room temperature absorption spectra by the following formula:

$$S_q^{meas}(J \rightarrow J') = \frac{3hc(2J+1)}{8\pi^3 e^2 \bar{\lambda} N} \frac{9n}{(n^2+2)^2} \int \alpha_q(\lambda) d\lambda \quad (2)$$

where the subscript q indicates the polarization of spectra, N is the concentration of Nd^{3+} ions in the sample, $\bar{\lambda}$ is the average wavelength of the absorption band, n is the refractive index, $\alpha_q(\lambda)$ is the absorption coefficient and $\int \alpha_q(\lambda) d\lambda$ is the integrated absorption coefficient for each absorption band.

According to J–O theory, the line strength of the electric-dipole transition can also be expressed as:

$$S_q^{cal}(J \rightarrow J') = \sum_{t=2,4,6} \left| \left\langle 4f^n[\alpha SL]J \left\| U^{(t)} \right\| 4f^n[\alpha' S' L']J' \right\rangle \right|^2 \quad (3)$$

where $\left\| U^{(t)} \right\|$ are the matrix element of unit tensor operators calculated by Carnall et al. [28].

The values of the measured line strengths with three polarizations are listed in Table 1. By a least-square fitting between Eqs. (2) and (3), the intensity parameters $\Omega_{2,4,6}$ with three polarizations are obtained and listed in Table 2. The effective intensity parameters, which are defined as $\Omega_{eff} = (\Omega_b + \Omega_{D1} + \Omega_{D2})/3$, are also listed in Table 2. The large value of Ω_2 mainly comes from the high absorption coefficient of the $^4I_{9/2} \rightarrow {}^4G_{5/2} + {}^2G_{7/2}$ hypersensitive transition around 585 nm [29,30]. This behavior has also been observed in some other molybdate crystals [14,15].

In order to justify the obtained results, the root-mean-square deviation of the experiment and calculation line oscillator strengths is introduced, which is defined by:

$$\text{rms}\Delta S_q = \sqrt{\frac{\sum_{i=1}^{N} (S_q^{meas} - S_q^{cal})^2}{N-3}} \quad (4)$$

where N is the number of experimental absorption bands. The measurement of the relative error is given by:

$$\text{rms error} = \frac{\text{rms}\,\Delta S}{\text{rms}\,S} \times 100\% \quad (5)$$

where

$$\text{rms}\,S = \sqrt{\frac{\sum_1^N S_{meas}^2}{N}} \quad (6)$$

Table 4
The spectral parameters of Nd^{3+}:$Li_3Ba_2Gd_3(MoO_4)_8$ and other Nd^{3+}-doped crystals.

Crystals		Nd^{3+}concentration (10^{-20}cm^{-3})	FWHM (nm)	σ_a ($\times 10^{-20}$ cm^2)	σ_e ($\times 10^{-20}$ cm^2)	τ_f (μs)	η (%)	Reference
$Nd^{3+}Li_3Ba_2Gd_3(MoO_4)_8$	E//b		6	15.13	9.5			
	E//$D1$	3.3	11	3.84	8.2	130	93	This work
	E//$D2$		8	5.27	7.9			
Nd^{3+}:$KLa(MoO_4)_2$	π	2.9	5	11.4	9.7	147	93	[34]
	σ				7.7			
Nd^{3+}:$PbWO_4$	π	1.2	5	14.83	11.9	132	98	[35]
	σ		5	3.32	5.5			
YVO_4	π	1.25	2	29.6	141	84	87	[24]
	σ			8.0	29.5			
$YAl_3(BO_3)_4$	π	3.11		0.94	13.7	302	18	[36,37]
	σ		7	2.58	9.7			

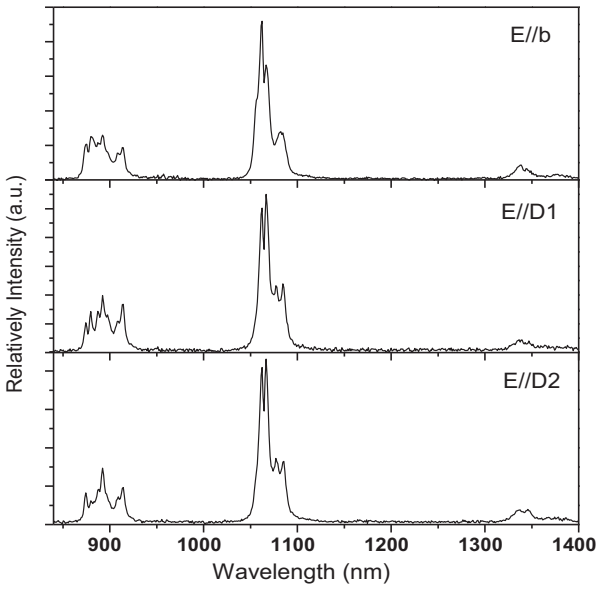

Fig. 8. Polarized fluorescence spectra of Nd^{3+}:$Li_3Ba_2Gd_3(MoO_4)_8$ crystal excited with 807 nm radiation at room temperature.

The value of the rmsΔS and rms error are in the typical error range of J–O fitting and indicate good agreement between the calculated and experimental results.

Once the J–O intensity parameters have been obtained, the spontaneous emission probability A from the initial multiplet $^4F_{3/2}$ to the terminal multiplet $^4I_{J'}$ (J' = 9/2, 11/2, 13/2 and 15/2) can be calculated by:

$$A_q(J \to J') = \frac{64\pi^4 e^2}{3h(2J+1)\bar{\lambda}^3} \frac{n(n^2+2)^2}{9} \sum_{t=2,4,6} \Omega_{tq} \left| \left\langle {}^4F_{3/2} \left\| U^t \right\| 4I_{J'} \right\rangle \right| \quad (7)$$

where $\left| \left\langle {}^4F_{3/2} \left\| U^t \right\| {}^4I_{J'} \right\rangle \right|$ were given by Kaminski [31] and $\bar{\lambda}$ is the mean wavelength of the fluorescence band. Then, the fluorescence branching ratio β is defined as:

$$\beta_q(J \to J') = \frac{A_q(J \to J')}{\sum_{J'} A_q(J \to J')} \quad (8)$$

The calculated values of A_q and β_q for the transitions from the $^4F_{3/2}$ multiplet are listed in Table 3.

The radiative lifetime τ_{rad} of a multiplet is the reciprocal of the total spontaneous emission probabilities from the multiplet. For an anisotropic crystal, the total spontaneous emission probabilities are expressed as:

$$A_{total} = \frac{\sum_q \sum_{J'} A_q(J \to J')}{3} \quad (9)$$

So, the radiative lifetime of the $^4F_{3/2}$ multiplet of Nd^{3+} ions in the Nd^{3+}:$Li_3Ba_2Gd_3(MoO_4)_8$ crystal is calculated to be 140 μs.

3.4. Fluorescence spectra and lifetime

Fig. 8 shows the polarized fluorescence spectra of the Nd^{3+}:$Li_3Ba_2Gd_3(MoO_4)_8$ crystal excited with 807 nm radiation. Three emission bands corresponding to the $^4F_{3/2} \to {}^4I_{9/2}$, $^4F_{3/2} \to {}^4I_{11/2}$ and $^4F_{3/2} \to {}^4I_{13/2}$ transitions are observed at 860–940, 1036–1120 and 1320–1405 nm. The emission cross-sections can be calculated from the fluorescence spectra using the Füchtbauer–Ladenburg (F–L) formula [32,33]:

$$\sigma_q^{F-L}(\lambda) = \frac{\lambda^5 A_q(J \to J') I_q(\lambda)}{8\pi c n^2 \int \lambda I_q(\lambda) d\lambda} \quad (10)$$

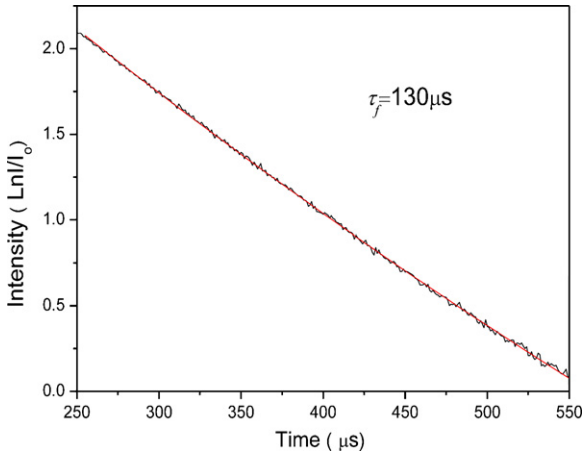

Fig. 9. Fluorescence decay curve of Nd^{3+} in Nd^{3+}:$Li_3Ba_2Gd_3(MoO_4)_8$ crystal.

where c is the speed of light in the vacuum, $I_q(\lambda)$ is the relative fluorescence intensity at wavelength λ and n is the refractive index. Then, the emission cross-sections σ_{em} for three polarizations are obtained and listed in Table 4.

The fluorescence lifetime decay curve of the $^4F_{3/2}$ multiplet is shown in Fig. 9. The fluorescence lifetime τ_f was determined to be 130 μs by linear fitting. Thus, the quantum efficiency η ($\eta = \tau_f/\tau_{rad}$) of Nd^{3+} in the Nd^{3+}:$Li_3Ba_2Gd_3(MoO_4)_8$ crystal was estimated to be 93%. Such high quantum efficiency can be mainly ascribed to the relatively low phonon energy of $[MoO_4]^{2-}$ group. As well known, the nonradiative transition rate from the excited multiplet to the next lower multiplet is mainly caused by the multi-phonon relaxation. The smaller the phonon energy is, the lower the nonradiative transition rate is. In the Nd^{3+}:$Li_3Ba_2Gd_3(MoO_4)_8$ crystal, the phonon energy of $(MoO_4)^{2-}$ group is generally bellow 900 cm^{-1}. Therefore, the nonradiative transition rate in the Nd^{3+}:$Li_3Ba_2Gd_3(MoO_4)_8$ crystal is relatively small and the quantum efficiency is high.

4. Conclusions

Nd^{3+}:$Li_3Ba_2Gd_3(MoO_4)_8$ crystal with dimensions of $25 \times 15 \times 10\,mm^3$ has been successfully grown by TSSG method and its spectroscopic properties were analyzed by J–O theory. The main spectroscopic parameters of Nd^{3+}:$Li_3Ba_2Gd_3(MoO_4)_8$ crystal are shown in Table 4 and compared with those of other Nd^{3+}-doped crystals. It can be found that the Nd^{3+}:$Li_3Ba_2Gd_3(MoO_4)_8$ crystal has a large FWHM at 805 nm, which is suitable for diode-laser pumping. The absorption and emission cross-sections of Nd^{3+}:$Li_3Ba_2Gd_3(MoO_4)_8$ crystal are smaller than that of Nd^{3+}:YVO_4, but larger than most of other reported Nd^{3+}-doped crystals. Moreover, it is remarkable that the Nd^{3+}:$Li_3Ba_2Gd_3(MoO_4)_8$ crystal has a high quantum efficiency η of 93%. In conclusion, Nd^{3+}:$Li_3Ba_2Gd_3(MoO_4)_8$ crystal may be regarded as a promising solid-state laser material for diode-laser pumping.

Acknowledgements

This project was supported by the Science Foundation of Shandong Province (ZR2009BM041 & ZR2010EQ007) and the Natural Science Foundation of the Anhui Higher Education Institutions of China (Grant No. KJ2010B203).

References

[1] X.M. He, L.H. Zhang, G.Z. Chen, Y. Hang, J. Alloys Compd. 467 (2009) 366–369.

[2] E. Cavalli, G. Calestani, A. Belletti, M. Bettinelli, A. Speghini, Opt. Mater. 31 (2009) 1340–1342.
[3] A. Majchrowski, S. Klosowicz, L.R. Jaroszewicz, M. Swirkowicz, I.V. Kityk, M. Piasecki, M.G. Brik, J. Alloys Compd. 491 (2009) 26–29.
[4] H. Li, L.Z. Zhang, Z.B. Lin, G.F. Wang, J. Alloys Compd. 493 (2010) 372–375.
[5] N. Jaba, M. Ajroud, G. Panczer, M. Férid, H. Maaref, Opt. Mater. 32 (2010) 479–483.
[6] Q. Dong, G.J. Zhao, D.H. Cao, J.Y. Chen, Y.C. Ding, J. Alloys Compd. 493 (2010) 661–665.
[7] A.S. Aleksandrovsky, I.A. Gudim, A.S. Krylov, A.V. Malakhovskii, V.L. Temerov, J. Alloys Compd. 496 (2010) L18–L21.
[8] M. Derbal, D. Ouadjaout, F. Siserir, V. Jubera, J.P. Chaminade, A. Garcia, O. Viraphong, M. Kadi Hannifi, Opt. Mater. 32 (2010) 756–758.
[9] A. Wojciechowski, M. Swirkowicz, A. Karas, L.R. Jaroszewicz, A. Majchrowski, E. Gondek, K. Ozga, I.V. Kityk, J. Alloys Compd. 504 (2010) 197–200.
[10] S.S. Cheng, X.D. Xu, D.Z. Li, D.H. Zhou, F. Wu, Z.W. Zhao, J. Xu, J. Alloys Compd. 506 (2010) 513–515.
[11] V. Volkov, C. Cascales, A. Kling, C. Zaldo, Chem. Mater. 17 (2005) 291–300.
[12] H.M. Zhu, Y.F. Lin, Y.J. Chen, X.H. Gong, Q.G. Tang, Z.D. Luo, Y.D. Huang, J. Appl. Phys. 102 (2007) 063104–063111.
[13] H.M. Zhu, Y.J. Chen, Y.F. Lin, X.H. Gong, Z.D. Luo, Y.D. Huang, J. Opt. Soc. Am. B 24 (2007) 2659–2665.
[14] X.Y. Huang, G.F. Wang, J. Alloys Compd. 475 (2009) 693–697.
[15] Y.W. Wei, Y.J. Chen, Y.F. Lin, X.H. Gong, Z.D. Luo, Y.D. Huang, J. Alloys Compd. 484 (2009) 529–534.
[16] W. Zhao, L.Z. Zhang, G.F. Wang, J. Cryst. Growth 311 (2009) 2336–2340.
[17] A. García-Cortés, C. Cascales, Chem. Mater. 20 (2008) 3884–3891.
[18] A. García-Cortés, C. Cascales, C. Zaldo, Mater. Sci. Eng. B 146 (2008) 89–94.
[19] M.J. Song, L.Z. Zhang, G.F. Wang, J. Alloys Compd. 480 (2009) 839–842.
[20] M.J. Song, G.J. Wang, Z.B. Lin, L.Z. Zhang, G.F. Wang, J. Cryst. Growth 308 (2007) 208–212.
[21] Y. Cheng, H. Zhang, Y. Yu, Z. Ling, X. Cheng, J. Wang, H. Xia, M. Jiang, Phys. B 383 (2006) 213–218.
[22] H.J. Zhang, L. Zhu, X.L. Meng, Z.H. Yang, C.Q. Wang, W.T. Yu, Y.T. Chow, M.K. Lu, Cryst. Res. Technol. 34 (1999) 1011–1016.
[23] J.J. Carvajal, R. Sole, J. Gavalsa, J. Massons, F. Diaz, M. Aguilo, Chem. Matter 15 (2003) 2730–2736.
[24] Y. Sato, T. Taira, IEEE J. Sel. Top Quantum Electron 11 (2005) 613–620.
[25] J. Lu, M. Prabhu, J. Song, C. Li, J. Xu, K. Ueda, A.A. Kaminskii, H. Yagi, T. Yanagitani, Appl. Phys. B 71 (2000) 469–473.
[26] B.R. Judd, Phys. Rev. 127 (1962) 750–761.
[27] G.S. Ofelt, J. Chem. Phys. 37 (1962) 511–520.
[28] W.T. Carnall, P.R. Fields, K. Rajnak, J. Chem. Phys. 49 (1968) 4424–4442.
[29] S. Tannabe, T. Ohyagi, N. Soga, T. Hanada, Phys. Rev. B 46 (1992) 3305–3310.
[30] L.H.C. Andrade, D.R. Ardila, J.P. Andreeta, M.S. Li, Opt. Mater. 22 (2003) 369–375.
[31] A.A. Kaminski, Laser Crystals, Their Physics and Properties, vol. 14, 2nd edition, Springer, Berlin, Heidelberg, 1990 (Springer Ser. Opt. Sci.).
[32] B.F. Aull, H.P. Jenssen, IEEE J. Quantum Electron 18 (1982) 925–930.
[33] D.E. McCumber, Phys. Rev. 136A (1964) 954–957.
[34] E. Cavalli, E. Zannoni, C. Mucchino, J. Opt. Soc. Am. B 16 (1999) 1958–1965.
[35] Y. Chen, Y. Lin, Z. Luo, Y. Huang, J. Opt. Soc. Am. B 22 (2005) 898–904.
[36] D. Jaque, J. Capmany, Z.D. Luo, J. Garcia Sole, J. Phys. Condens. Matter 9 (1997) 9715–9729.
[37] D. Jaque, J. Capmany, J.A. Sanz Garcia, A. Brenier, G. Boulon, J. Garcia Sole, Opt. Mater. 13 (1999) 147–157.